Hindawi
Advances in Multimedia
Volume 2022, Article ID 9467820, 11 pages
https://doi.org/10.1155/2022/9467820

Research Article

Appearance Design Method of Smart Street Lamp Based on Kansei Engineering

Junchao Ge[1,2] **and Lipeng Wang**[1]

[1]*Hebi Institute of Engineering and Technology, Henan Polytechnic University, Jiaozuo, Henan 454000, China*
[2]*Faculty of Engineering, Built Environment and Information Technology-SEGi University, Kota Damansara, Selangor Darul Ehsan 47810, Malaysia*

Correspondence should be addressed to Junchao Ge; gejunchao@hpu.edu.cn

Received 17 May 2022; Revised 4 June 2022; Accepted 20 June 2022; Published 9 July 2022

Academic Editor: Qiangyi Li

In order to improve the scientificity of the appearance design of smart street lamps, this paper studies the appearance design method of smart street lamps combined with Kansei engineering so as to improve the appearance design effect of street lamps. Moreover, this paper optimizes the design of free-form surface optical light distribution, microlens array to improve the light extraction efficiency of high-power smart street lamps, and the heat dissipation structure of lamps. In addition, in view of the shortcoming that the direct design of free-form surface lenses for smart street lamps is not widely applicable, this paper proposes the concept of integration of microlens array packaging for smart street lamps. Finally, this paper verifies that the intelligent street lamp design based on Kansei engineering meets the lighting needs through experimental research. Through the experimental evaluation, it can be seen that the appearance design method of smart street lamps based on Kansei engineering proposed in this paper can effectively improve the structural performance of street lamps.

1. Introduction

Compared with ordinary street lights, smart street lights have a more complex structure. In the design stage, in addition to the lighting effect, energy consumption cost, and decorative effect of street lights, the structural safety of smart street lights is also an important issue. In areas with strong wind, the new energy panels, batteries, and charge and discharge controllers of smart street lamps occupy a large space. In the event of extreme weather, such as strong typhoons, the failure of smart street lights often occurs due to insufficient structural strength. These damages caused by insufficient wind resistance will bring great harm to people's life and property safety. Therefore, whether the structural design is reasonable is the main issue affecting its structural safety. The finite element analysis of the structure can provide a reliable design basis for further structural design, and at the same time, it can effectively reduce the research and development cost of smart street lamps, which has certain engineering practical significance.

The reason for designing the components of the smart street light is that the power of the smart street light battery board directly affects the wind resistance of the overall structure, and the size of the lithium battery capacity affects the overall gravity of the smart street light itself. Moreover, the power of the LED lamp directly affects the power of the required new energy battery panel and the capacity of the lithium battery [1]. Important functional components of smart street lights include new energy battery panels, LED lights, charge and discharge controllers, and lithium batteries. This study does not involve circuit control, so the design study of the charge-discharge controller is not carried out. The type of new energy battery panel is a single crystal silicon new energy battery with a high conversion rate in the market. The required power is affected by the power of the LED lamp. Therefore, the power of the LED lamp should be determined first in the design calculation. At the same time, the power of LED lights is affected by specific road lighting standards, so it is necessary to first calculate the power of LED lights according to the lighting standards of urban

roads. The type of lithium battery is tentatively set as lithium iron phosphate battery, and the size of its electric capacity needs to be determined in combination with the power of the LED lamp and the relevant meteorological data of the installation site [2].

Compared with other structures in smart street lights, although the structure of the light pole is relatively simple, the light pole is the component with the largest load in the overall structure. When encountering extreme weather, such as strong convection, the light pole will yield due to insufficient structural strength. The probability of failure is greater, and the damage caused by the failure of the light pole due to insufficient strength is also greater [3]. The calculation of the strength and deflection of the light pole belongs to the analysis and calculation of statics, and the relevant theoretical knowledge of the third strength theory and material mechanics will be used in the calculation process. In the actual environment, the fluctuation of wind force often causes the resonance of the structure, so the calculation of the natural frequency of the light pole is also very important. The natural frequency of the light pole with simple structure can be calculated by the Euler–Bernoulli beam theory [4].

The controller of the smart street light is the core device of the smart street light, which is responsible for completing the functions of charge and discharge control and management. At present, developed countries, such as the United States, Germany, and other countries are committed to improving the output power of new energy batteries, lithium battery charging strategies, and system stability research. The controller has developed from the simple realization of the charging and discharging control function of lithium batteries in the early days to the use of microprocessors to realize software programming and develop in the direction of intelligence [5]. Literature [6] proposes a "three-stage" control charging method for smart street lamp battery charging based on the charging characteristics of the battery and the output characteristics of the new energy battery. In different stages, different state modes of new energy battery maximum power output charging, constant voltage current limiting, and floating charging are used; for battery discharge protection, the output mode is adjusted in real time through the detection of battery remaining capacity, and when necessary, the action of stopping the power supply to the load. Literature [7] analyzes the output characteristics of new energy batteries and analyzes and compares several commonly used maximum power point tracking (MPPT) algorithms. On the basis of summarizing their advantages and disadvantages, a maximum power control scheme LCMPPT is proposed. The method achieves the purpose of maximum power tracking by setting an error limit so that the output of the new energy battery always oscillates near its maximum power point. Literature [8] designed an intelligent LED intelligent street light control system. The system is based on ATmegal6 single-chip microcomputer, which realizes the detection of the voltage and current of new energy photovoltaic cells and batteries, the control of battery charging and LED drive circuits, and the remote communication function, which can control or detect each street light; it is convenient for managers to control and maintain the street lights. Literature [9] designed an intelligent street lamp controller for the problem that the domestic intelligent street lamp controller in the market is not highly intelligent and cannot effectively protect the battery.

When designing a light pole or a new energy board bracket, the reliability of the designed structure must be considered. Due to limited test conditions and various practical problems, some manufacturers often only use a larger safety factor based on previous design experience and ignore specific research on structural reliability, which often leads to unreasonable structural design of smart street lamps, which will not only reduce the product, but will bring great safety hazards to pedestrians and vehicles on the road [10]. The use of finite element software to simulate related structures has attracted more and more attention. Compared with the physical test, the advantage of finite element simulation analysis is that it can save time and cost, and the simulation analysis results are also quite accurate [11]. Literature [12] used theoretical calculation and finite element method to analyze the natural frequency, strength, and stiffness of high pole lights. The calculation results of the two methods are compared, and it is shown that the theoretical calculation and the finite element analysis are basically consistent with the natural frequencies of each order, the strength of the dangerous section of the pole, and the maximum deflection of the three-section pole. The finite element calculation also calculates the stress value of the rib, flange, lamp frame, and other structures whose strength is difficult to obtain through theoretical calculation. This shows the superiority of finite element calculation over theoretical calculation. Literature [13] used the finite element software Ansys to obtain the stress and displacement of the light pole through the finite element analysis of the 8 m aluminum alloy light pole under the action of wind load and its own gravity and verified the validity of the finite element model through experimental tests. Literature [14] studied the mechanical properties and vibration characteristics of a certain type of wind-solar hybrid street light by means of theoretical calculation and finite element software Ansys simulation analysis, verified the accuracy of the finite element analysis results, and put forward suggestions for structural improvement accordingly.

Literature [15] used life cycle assessment (LCA) to evaluate and compare two street lighting technologies in Lebanon from an environmental perspective, a traditional grid-connected system and a new energy independent system, and found that when considering landfill and recycling, the new energy system, the overall environmental impact is much smaller. Literature [16] uses new energy technology as a replacement for the original street and park lighting. After budgeting, it is found that new energy technology can completely solve the power supply problem of the street and park lighting system caused by the lack of electricity from the national power company. Literature [17] used the maximum power point tracking technology (MPPT) and used the perturbation and observation algorithm to design the charging circuit and developed an LED driver circuit for this system. Literature [18] arranges

multiple vertical axis wind turbines into the structure itself of the lamp post and combines photovoltaic panels to generate electricity, and the energy is collected through power conversion equipment together with storage equipment to ensure lighting during windless nights. The safety equipment is used to prevent the turbine from overspeeding by automatically stopping in extreme wind conditions. Literature [19] applied the wireless sensor network to the wind-solar hybrid street lamps and adopted ZigBee technology to realize the communication between the street lamps and realize the real-time monitoring of the wind-solar hybrid street lamps. Literature [20] designed a special dust cleaning circuit in the smart street light system to regularly reduce the amount of dust covered on the new energy panel and improve the overall system efficiency. Literature [21] designed a new type of new energy smart street light, which has an energy management algorithm, which can automatically estimate the new energy stored in the battery, determine the night time, and control the intensity of the street light to effectively utilize the stored energy and improve energy efficiency and energy utilization of the whole system.

This paper studies the appearance design method of smart street lamps combined with Kansei Engineering, improves the appearance design effect of street lamps, and improves the structure and scientificity of street lamps.

2. Appearance Design Algorithm of Smart Street Lamp

2.1. Nonimaging Optics and Free-Form Surfaces. The relationship between the incident light, the outgoing light, and the free-form surface normal vector is established, as shown in Figure 1. According to the spatial refraction (Snel1) law, the following can be obtained.

$$n'\left(\overrightarrow{A_0'} \times \vec{N}\right) = n\left(\overrightarrow{A_0} \times \vec{N}\right). \tag{1}$$

Among them, n' and n are the refractive indices of the refracting medium and the incident medium, respectively, $\vec{N}$ is the normal vector, and $\overrightarrow{A_0'}$ and $\overrightarrow{A_0}$ are the unit vectors of the refracted and incident rays. When $\overrightarrow{A'} = n' \cdot \overrightarrow{A_0'}$ and $\overrightarrow{A'} = n \cdot \overrightarrow{A_0}$, the above formula can be transformed into

$$\left(\overrightarrow{A'} - \vec{A}\right) \times \vec{N} = 0. \tag{2}$$

Because the two vectors in the above formula cannot be zero at the same time, the above formula can be expressed as

$$\overrightarrow{A'} = \vec{A} + P\vec{N}. \tag{3}$$

Among them, $P = \sqrt{n'^2 - n^2 + n^2\cos^2 I} - n\cos I$. Converting (3) into scalar form and normalizing it, we get

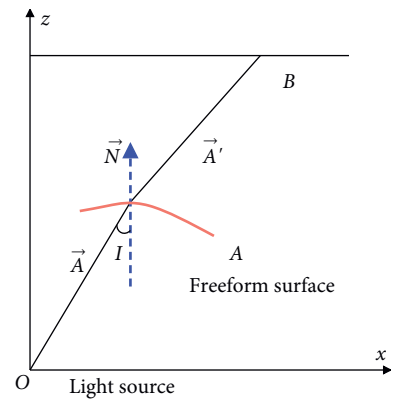

Figure 1: Schematic diagram of the law of spatial refraction.

$$\begin{cases} N_x = \dfrac{A_x' - A_x}{\sqrt{2}\sqrt{|\vec{A}|^2 - \vec{A'} \cdot \vec{A}}} \\ N_y = \dfrac{A_y' - A_x}{\sqrt{2}\sqrt{|\vec{A}|^2 - \vec{A'} \cdot \vec{A}}} \\ N_z = \dfrac{A_z' - A_x}{\sqrt{2}\sqrt{|\vec{A}|^2 - \vec{A'} \cdot \vec{A}}} \end{cases} \tag{4}$$

Therefore, under the condition that the incident ray vector and the refracted ray vector are known, the envelope surface of the free-form surface can be outlined by iteration.

As shown in Figure 2, a beam of light has a direction cosine (α, β) at point P with an area of $dxdy$, and the refractive index of the medium is n. After passing through the optical system and entering the medium with the refractive index j, the area and direction cosines of the microelements become $dx'dy'$ and (α', β'). If the optical system is lossless and etendue is conserved:

$$\begin{aligned} n^2 dxdyd\alpha d\beta = n'^2 dx'dy'd\alpha' d\beta' &= n^2 dAd\alpha d\beta \\ &= n^2 dA\cos\theta d\omega \end{aligned} \tag{5}$$

Among them, $dA = dx\,dy$ is the area of the surface element, θ is the angle between the z-axis and the normal direction of the surface element, and $d\omega$ is the solid angle. If we take $dp_x = n\,da$ and $dp_y = n\,d\beta$, we have

$$\begin{aligned} n^2 dxdyd\alpha d\beta = n'^2 dx'dy'd\alpha' d\beta' &= n^2 dAd\alpha d\beta \\ &= dxdydp_x dp_y \end{aligned} \tag{6}$$

The integral form of formula (6) is

$$\begin{aligned} \int n^2 dxdyd\alpha d\beta = \int n'^2 dx'dy'd\alpha' d\beta' &= \int n^2 dAd\alpha d\beta \\ &= \int dxdydp_x dp_y. \end{aligned} \tag{7}$$

The four values of the above formula are the etendue, which can be regarded as the extended form of the Lach invariant in three-dimensional space. The physical meaning of etendue conservation is that the luminous flux in the

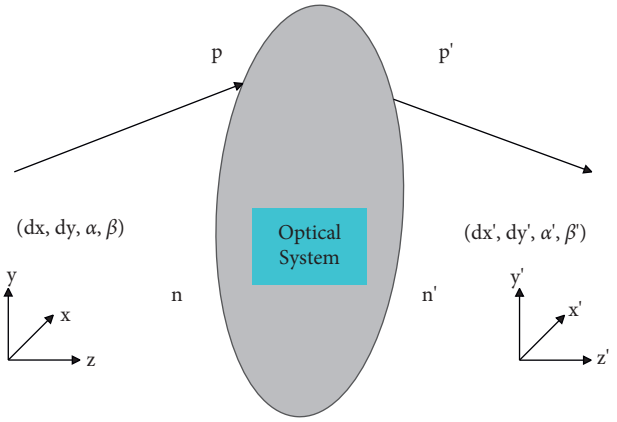

Figure 2: Etendue conservation of optics.

microelement $dxdy$ and solid angle $d\alpha\, d\beta$ remains unchanged during the propagation process without considering the energy loss, such as absorption, scattering, and reflection (the optical system is not damaged). This law is a universal law, which does not depend on the symmetry of the optical system or the uniformity of the refractive index, and can be proved by Liu Wei's theorem or the characteristic equation.

As shown in Figure 3, if the light source is a point light source located at the origin, and the corresponding light intensity of the propagation direction (θ, φ) in the spherical coordinate system is $I(\theta, \varphi)$, the radiant flux of the light source can be expressed as

$$\Phi_S = \int I(\theta, \varphi) d\Omega \tag{8}$$

Among them, $d\Omega$ is the unit solid angle, and the size is

$$d\Omega = r^2 \sin\theta\, d\theta d\varphi / r^2 = \sin\theta\, d\theta d\varphi \tag{9}$$

By substituting formula (9) into formula (8), we get

$$\int_0^{\theta} \int_0 I(\theta, \varphi) \sin\theta\, d\theta d\varphi = \int E(x, y, z) dA \tag{10}$$

Among them, $E(x, y, z)$ is the illuminance at the point (x, y, z), and dA is the target surface area. The specific form of the relationship equation between (θ, φ) and the illumination target surface is related to the topological relationship between the light source and the target surface, and only formula (10) cannot be obtained.

2.2. Mathematical Representation of Free-Form Surfaces. For Bézier splines, when the order is n,

$$B(t) = \sum_{i=0}^{n} B_{i,n}(t) P_i = \sum_{i=0}^{n} \frac{n!}{(n-i)!i!} t^i (1-t)^{n-i} P_i t \in [0,1]. \tag{11}$$

Among them, $P_i(P_1, P_2, \ldots P_n)$ is the control point of the curve. The formed polygon is used to approximate the shape of the curve well. The Bézier spline is essentially a polynomial representation, including quadratic curves such as ellipse and hyperbola, which can be represented by the quotient (rational function) of two polynomials. The nth-order Bézier spline is defined as

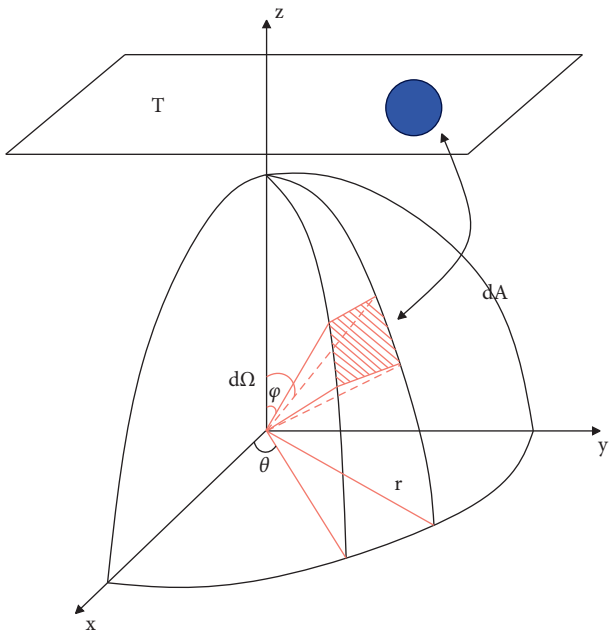

Figure 3: Topological relationship between the solid angle of the light source and the illumination target surface.

$$B(t) = \sum_{i=0}^{n} R_{i,n}(t) P_i = \sum_{i=0}^{n} \frac{w_i B_{i,n}(t)}{\sum_{j=0}^{n} w_j B_{j,n}(t)} P_i t \in [0,1]. \tag{12}$$

Among them, w_i is the weight factor, and by changing the value of w_i, we can get different free curves. By extending the Bézier spline to grid control points in two directions, the irrational Bézier spline surface and the rational Bézier spline surface can be obtained.

$$\begin{aligned} B(t,s) &= \sum_{j=0}^{m} \sum_{i=0}^{n} B_{i,n}(t) B_{j,m}(s) P_{i,j} \\ &= \sum_{j=0}^{m} \sum_{i=0}^{n} \frac{n!}{(n-i)!i!} \frac{m!}{(m-i)!ji} t^i (1-t)^{n-i} (1-s)^{m-i} P_{i,j} \end{aligned} \tag{13}$$

$$B(t,s) = \sum_{j=0}^{m} \sum_{i=0}^{n} \frac{B_{i,n}(t) B_{j,m}(s) w_{i,j}}{\sum_{k=0}^{n} \sum_{l=0}^{m} B_{k,n}(t) B_{l,m}(s) w_{k,l}} P_{i,j} t, s \in [0,1].$$

Among them, $P_{i,j}$ is the mesh control vertex of the surface.

We take a monotonically nondecreasing sequence of real numbers $T = \{t_0, t_1, \ldots, t_{i+n+1}\}$, where P_i is the control vertex, and there is a total of m. Then, the B-spline curve of order can be expressed as

$$B(t) = \sum_{i=0}^{m} B_{i,n}(t) P_i t \in [0,1]. \tag{14}$$

Among them, $N_{i,n}(t)$ represents the ith nth-order B-spline basis function, which is defined as

$$B_{i,n}(t) = \begin{cases} B_{i,0}(t) = \begin{cases} 1 & t_i \le t \le t_{i+1} \\ 0 & \text{other} \end{cases} \\ B_{i,n}(t) = \dfrac{t - t_i}{t_{i+n} - t_i} N_{i,n-1}(t) + \dfrac{t_{i+n+1} - t}{t_{i+n+1} - t_{i+1}} N_{i+1,n-1}(t) \end{cases} \tag{15}$$

If the control vertex k is uniformly spaced, formula (16) is a uniform B-spline curve; otherwise, it is a nonuniform B-spline curve. A big difference between B-splines and Bézier curves is their local support. If $Bt \notin (t_i, t_{i+n+1})$, then there is $B_{i,n}(t) = 0$. Such a local support makes the B-spline curve change the position of a certain control vertex; only the shape of the curve in the (t_i, t_{i+n+1}) interval is changed, and the shape of the curve in the other interval remains unchanged.

It extends to the two direction nodes of $T = \{t_0, t_1, \ldots, t_{n+k+1}\}$‘$S = \{s_0, s_1, \ldots, s_{m+l+1}\}$ and the control vertex $P_{i,j}$, where $i = 0 \sim m$ and $j = 0 \sim l$. At this time, the $n \times m$-order B-spline surface is

$$B(t,s) = \sum_{j=0}^{m} \sum_{i=0}^{n} B_{i,k}(t) B_{j,}(s) P_{i,j} t \in [u_k, u_{n+1}], s \in [s_l, s_{m+1}] \tag{16}$$

Combining the above related concepts, NURBS (non-uniform rational B-splines) curves can be obtained. When the node is $T = \{t_0, t_1, \ldots, t_{m+n+1}\}$ and the control vertex is $P_i\,(m+1)$, the nth-order NURBS curve is

$$B(t) = \frac{\sum_{i=0}^{m} w_i B_{i,n}(t)}{\sum_{j=0}^{m} w_j B_{j,n}(t)} P_i t \in [0,1]. \tag{17}$$

Among them, w_i is the weight factor, and the above formula can be written as

$$B(t) = \sum_{i=0}^{m} R_{i,n}(t) P_i t \in [0,1] \tag{18}$$

Among them, the rational B-spline basis function $R_{i,n}(t)$ of order n is

$$R_{i,n}(t) = \frac{w_i B_{i,n}(t)}{\sum_{j=0}^{m} w_j B_{j,n}(t)} t \in [0,1] \tag{19}$$

By changing the weight factor w_i and moving the control vertices, the shape of the NURBS curve can be changed so as to obtain rational and irrational Bézier curves and irrational B-spline curves.

A NURBS surface of order n in the t-direction and m-order in the s-direction can be expressed as

$$B(t,s) = \frac{\sum_{j=0}^{m} \sum_{i=0}^{n} B_{i,n}(t) B_{j,m}(s) P_{i,j} w_{i,j}}{\sum_{k=0}^{n} \sum_{l=0}^{m} B_{k,n}(t) B_{l,m}(s) w_{i,j}} t, s \in [0,1] \tag{20}$$

Rational basis functions are introduced:

$$R_{i,j}(t,s) = \frac{B_{i,n}(t) B_{j,m}(s) w_{i,j}}{\sum_{k=0}^{n} \sum_{l=0}^{m} B_{k,n}(t) B_{l,m}(s) w_{i,j}} t, s \in [0,1] \tag{21}$$

Formula (22) can be written as

$$B(t,s) = \sum_{j=0}^{m} \sum_{i=0}^{n} R_{i,j}(t,s) P_{i,j} t, s \in [0,1]. \tag{22}$$

2.3. Secondary Optical Light Distribution Design of High-Power Smart Street Lamps. In order to accurately obtain the uniform illumination of the illuminated target surface, an equal division method should be adopted for the grid division of the light space; that is, the light energy (flux) of each grid in the light space is the same. We assume that the ray space is divided into MxN parts of equal luminous flux. As shown in Figure 4, M is the vertical direction of the light space along the LED chip normal (horizontal, i is the horizontal index), and N is the light space along the normal direction of the LED chip (longitudinal, j is the vertical index). (I,j) is a node in the ray space and corresponds to the node of the target surface. When it is divided along the longitudinal direction, since the light space of the LED has rotational symmetry, it only needs to be evenly divided in the whole angle.

The LED light space in the horizontal direction is not symmetrical, and the division method is more complicated. The light space is cut into M parts with the same luminous flux in the horizontal direction.

$$\Phi = \Phi_{\text{total}} / M \tag{23}$$

In this way, M demarcation points in the transverse direction can be obtained.

Different energy mapping methods can be adopted for the division of pavement grids. Figure 5 shows a way of meshing the parallel lines of the pavement, and only one quadrant is drawn here. The luminous flux within the ray angle (θ, φ) and the solid angle $d\Omega$ is mapped to the rectangular surface element of the target surface through the free-form surface. In this mapping relationship, the surfels of the illumination target surface along the x-axis direction correspond to the grid of the same θ angle in the light space, and the surfels along the y-axis direction correspond to the grid of the same φ angle of the light space. The light intensity distribution in the light space is

$$I(\theta, \varphi) = I_0 \sin\theta \cos\varphi \tag{24}$$

We substitute formula (25) into formula (9). According to the law of conservation of energy,

$$\int_0^{\theta} \int_0^{\infty} I_0 \sin^2\theta \cos\varphi \, d\theta d\varphi = \iint E(x,y) dA \tag{25}$$

By taking the street lamp interval and road width as L and W, respectively, the corresponding relationship between x and θ can be determined:

$$I_0 \int_0^{\pi/2} \cos\varphi \, d\varphi \int_b^{\pi/2} \sin^2\theta \, d\theta = ExLx = \frac{1}{4} \frac{I_0 [\pi - (2\theta - \sin(2\theta))]}{EL} \tag{26}$$

Similarly,

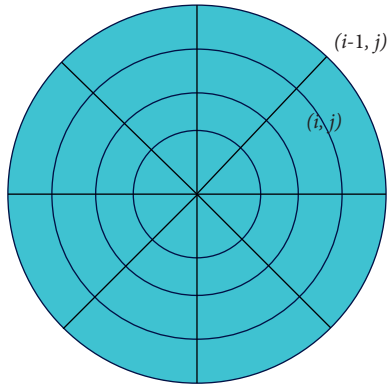

Figure 4: Isometric meshing of ray space.

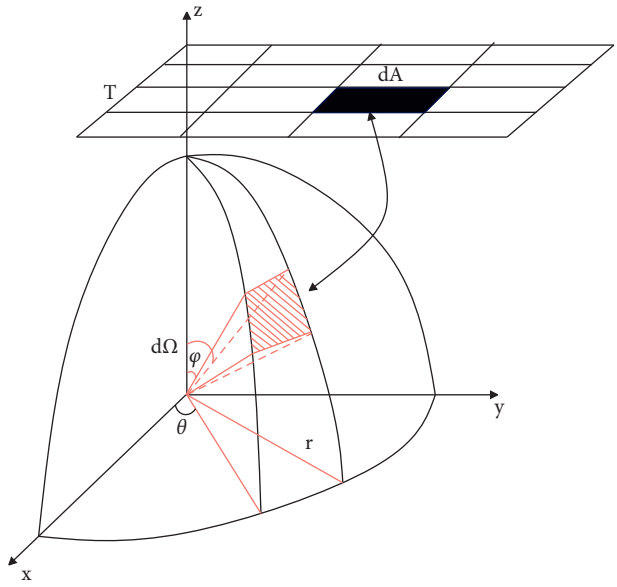

Figure 5: Schematic diagram of grid division of parallel line planes.

$$I_0 \int_0 \cos\varphi \, d\varphi \int_0^{\pi/2} \sin^2\theta \, d\theta = EyWy = \frac{1}{4} \frac{\pi I_0 \sin \varphi}{EW} \tag{27}$$

This division method is relatively simple, but there is a problem. As shown in Figure 6, the light space and road surface are divided into 3×4 parts. The intersection of the ray space grid curve and the curve, the curve and the coordinate axis represents a ray, and the intersection between the road grid lines, the line, and the coordinate axis represents the landing point of the ray. Obviously, the ray space grid contains 16 rays, while the pavement grid has 20 drop points. Most of the rays and the landing points satisfy a one-to-one correspondence. However, the ray along 0 = 0 corresponds to all the landing points of $x = L$, and the light along enough = 0 corresponds to all the landing points of $Y=W$. This results in that multiple different normal vectors correspond to a point on the free-form surface, which is inconsistent with the actual situation.

Figure 7 shows another schematic diagram of radial grid division of pavement, which also only takes one quadrant. The luminous flux within the ray angle (θ, φ) and the solid angle $d\Omega$ is mapped to the dA trapezoidal surface element of the target surface through the free-form surface. The road surface is divided into $M \times N$ grids, and each ray subspace corresponds to a specific grid of the road surface. Obviously, in order to get uniform illumination on the road, the distribution of the road grid is equal area. As shown in Figure 8, the road surface is meshed in a radial manner.

First, we divide the rectangular pavement into n parts with the same area and assume that the length and width of the pavement are $L = x(n)$ and $W = y(n)$, respectively. Therefore, the aspect ratio is $a = L/W$, the pavement area is $S = L.W$, and it can be obtained as

$$S_1 = S_2 = S_3 = \cdots = S/n \tag{28}$$

$$\begin{cases} S_1 = S/n \\ S_2 = x(2) \cdot y(2) - S_1 \\ \cdots \\ S_i = x(i) \cdot y(i) - x(i-1) \cdot y(i-1) \\ \cdots \\ S_n = x(n) \cdot y(n) - x(n-1) \cdot y(n-1) \end{cases} \tag{29}$$

$x(i)$ and $y(i)$ can be obtained by formulas (28) and (29). Then, we divide each subregion into m parts of equal area. It can be seen from the figure that

$$\frac{\Delta x_i(n-1)}{\Delta x_i(n)} = \frac{y(n-1)}{y(n)} = \frac{x(n-1)}{x(n)} \tag{30}$$

Therefore, for each i, there are $\Delta x_i(n) = \Delta x_i(n-1)$ and $\Delta y_i(n) = \Delta y_i(n-1)$, and $\alpha \Delta y_i(n) = \Delta x_i(n)$; the coordinates of the four corners of each road grid can be obtained. According to the edge ray theory, the light emitted from the edge of the light source can also irradiate the edge of the illumination target surface, and the light inside the light source can also irradiate the target surface. In the case of 3D, by increasing the number of grids $M \times N$, a more accurate correspondence can be achieved. For the four rays in the four corners of the ray space surface element in Figure 7, make sure that they fall on the four corners of the target surface dA surface element after passing through the free-form surface. However, in the central area of the light source, the three grid points between them are expected to correspond. In this way, the ray space that has been divided into MXN grids can be in one-to-one correspondence with the grid points on the target surface. That is, each ray emitted by the light source corresponds to a grid point on the target surface.

As shown in Figure 9, the incident ray $\vec{A}$ is refracted into ray $\vec{A}'$ at the point P. According to formula 4, the normal vector $\vec{N}$ of point P and the tangent plane can be calculated, and $\vec{B}$ is the adjacent ray of $\vec{A}$, which intersects the tangent plane of point P at point Q. If the distance between the two rays of $\vec{A}$, $\vec{B}$ is close enough, the Q point can be considered as the adjacent point to the P point on the free-form surface,

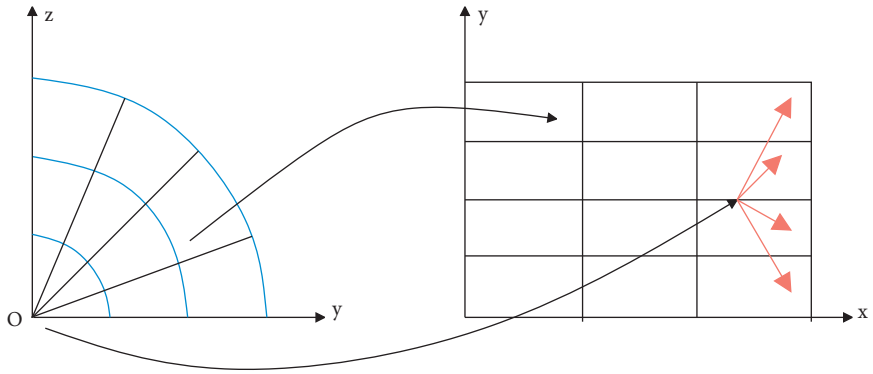

Figure 6: Defects in the meshing of parallel lines.

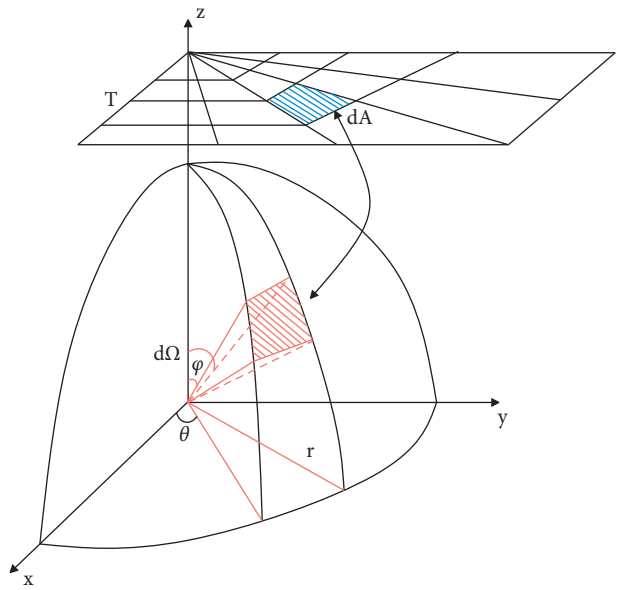

Figure 7: Schematic diagram of radial pavement meshing.

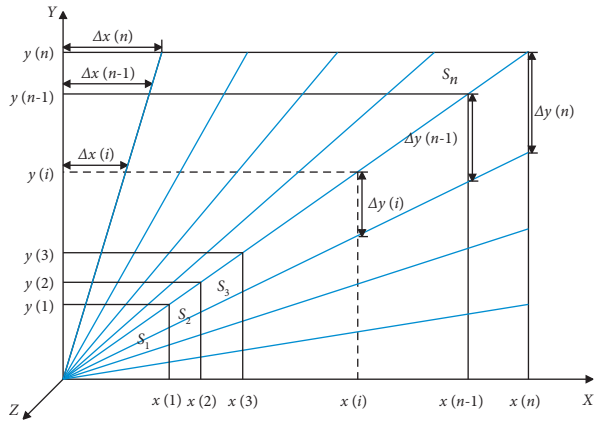

Figure 8: The division of the road grid.

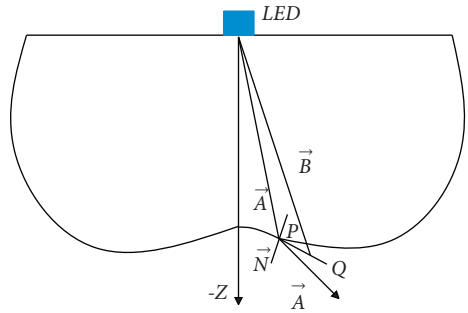

Figure 9: Principle of ray tracing.

and the entire free-form surface can be obtained after iteration. Principle of ray tracing is shown in Figure 9.

The spatial coordinate of point P is $(x_P(i,j), y_P(i,j), z_P(i,j))$, where i and j are the horizontal and vertical index marks, respectively, and the tangent plane of this point can be obtained as

$$\begin{aligned} &N_x(i,j)\left(x - x_P(i,j)\right) + N_y(i,j)\left(y - y_P(i,j)\right) \\ &+ N_z(i,j)\left(z - z_P(i,j)\right) = 0 \end{aligned} \tag{31}$$

Among them, $N_x(i,j), N_y(i,j)$, and $N_z(i,j)$ are the normal vector components of point P, and (x, y, z) are the coordinates of any point in the tangent plane. From the horizontal iterative algorithm, it can be known that the $\vec{B}$-line equation is

$$\begin{aligned} \frac{x}{\sin\varphi(i+1,j)\cos\theta(i+1,j)} &= \frac{y}{\sin\varphi(i+1,j)\sin\theta(i+1,j)} \\ &= \frac{z}{\cos\varphi(i+1,j)}. \end{aligned} \tag{32}$$

Combining formulas (31) and (32), the Q-coordinate of the intersection of $\vec{B}$ and the tangent plane can be obtained:

$$\begin{cases} x_Q(i,j+1) = \dfrac{N_x(i,j)\cdot x_P(i,j) + N_y(i,j)\cdot y_P(i,j) + N_z(i,j)\cdot z_P(i,j)}{N_x(i,j) + \tan\theta(i,j+1)\cdot N_y(i,j) + \cot\varphi(i,j+1)\cdot N_z(i,j)/\cos\theta(i,j+1)} \\ y_Q(i,j+1) = x_Q(i,j+1)\cdot \tan\theta(i,j+1) \\ z_Q(i,j+1) = x_Q(i,j+1)\cdot \cot\varphi(i,j+1)/\cos\theta(i,j+1) \end{cases}. \tag{33}$$

If the longitudinal iterative algorithm is used, formulas (32) and (33) become

$$\frac{x}{\sin\varphi(i,j+1)\cos\theta(i,j+1)} = \frac{y}{\sin\varphi(i,j+1)\sin\theta(i,j+1)} = \frac{z}{\cos\varphi(i,j+1)}$$

$$\begin{cases} x_Q(i,j+1) = \dfrac{N_x(i,j)\cdot x_P(i,j) + N_y(i,j)\cdot y_P(i,j) + N_z(i,j)\cdot z_P(i,j)}{N_x(i,j) + \tan\theta(i,j+1)\cdot N_y(i,j) + \cot\varphi(i,j+1)\cdot N_z(i,j)/\cos\theta(i,j+1)}, \\ y_Q(i,j+1) = x_Q(i,j+1)\cdot \tan\theta(i,j+1), \\ z_Q(i,j+1) = x_Q(i,j+1)\cdot \cot\varphi(i,j+1)/\cos\theta(i,j+1). \end{cases} \tag{34}$$

Obviously, when different iterative algorithms are used, the obtained free-form surfaces are also different.

3. Design Examples and Analysis

The secondary optical light distribution design commonly used in smart street lamps is divided into two types: reflector and lens. The reflector is relatively simple to process and the

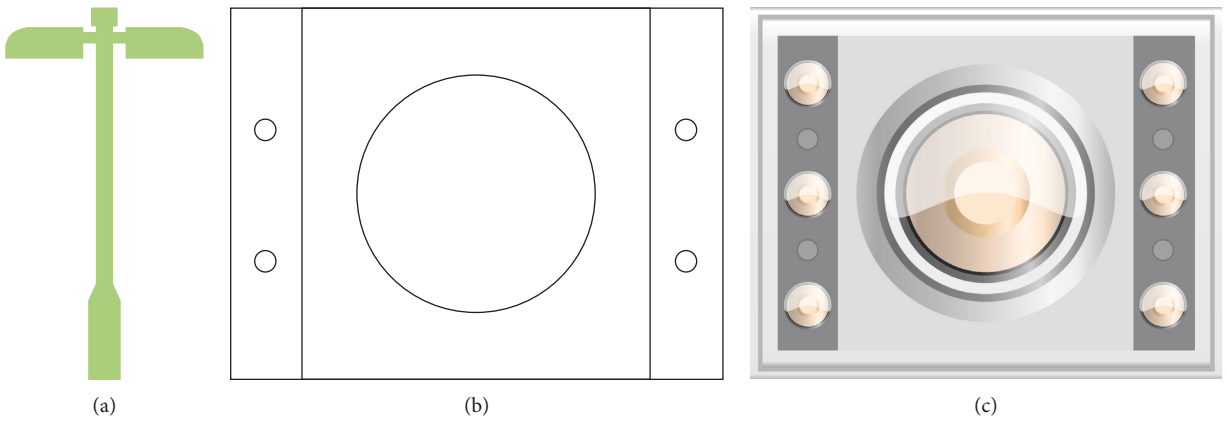

Figure 10: Design renderings of smart street lamps based on Kansei engineering. (a) Appearance of main structure of street lamp. (b)Preliminary design of lamp body structure. (c)Design effect of lamp body structure.

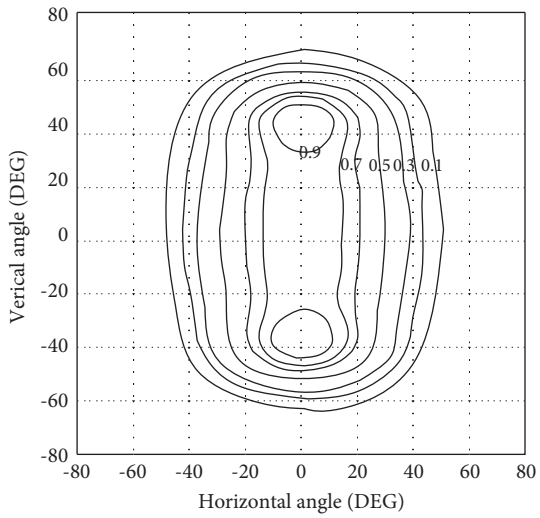

Figure 11: Isoluminous intensity curves of lamps.

cost is low, and the light is directly directed to the road after one reflection, and the energy loss is small. However, the reflector is generally aimed at a single LED chip, and the smart street lamp is a series of multiple chips to form a module, and then multiple modules form a street lamp. In this paper, in order to reduce the amount of calculation and processing cost, one side of the free-form lens is spherical, and the other is free form. Moreover, the light emitted by the LED located at the spherical center of the first surface enters the lens without refraction and is refracted on the free-form surface of the second surface after passing a certain optical path and forms a rectangular light spot with uniform illumination on the road surface.

Based on Kansei engineering, the appearance of the smart street lamp designed in this paper is shown in Figure 10.

Figure 11 shows the measured iso-intensity curve. Along the road and perpendicular to the road, the light is basically limited within the range of ±62° and ±40°, which is in good agreement with the edge of the designed road. The light energy utilization rate in the 30 m × 13 m area under the street lamp is 91.3%, the average illuminance in the horizontal and vertical directions is 31.171x and 25.721x, and the uniformity of the illuminance is 82.4% and 77.6%, respectively.

The above verifies that the intelligent street lamp design based on perceptual engineering proposed in this paper meets the lighting needs, and on this basis, the structure of the street lamp designed in this paper needs to be analyzed.

The wind vibration response analysis of the structure is closely related to the dynamic characteristics of the structure. The premise of the wind vibration response analysis in ABAQUS is the modal analysis. The dynamic characteristics of the structure include natural frequency, mode shape, and damping ratio, and modal analysis using finite element is an effective way to obtain these parameters. In ABAQUS, there

Table 1: Performance evaluation of the appearance design structure of smart street lamps based on Kansei engineering.

No.	Structural properties
1	88.92
2	88.58
3	88.90
4	93.33
5	87.53
6	93.60
7	89.51
8	87.72
9	90.10
10	90.80
11	88.67
12	89.86
13	88.42
14	92.99
15	89.56
16	87.96
17	89.47
18	87.63
19	87.67
20	89.43
21	91.87
22	87.91
23	93.92
24	87.73
25	93.31
26	91.93
27	87.72
28	91.04
29	90.91
30	93.43
31	91.55
32	93.61
33	92.69
34	89.90

are three conventional methods for extracting modes, including Lanczos method, Subspace method, and Automatic Multilevel Substructuring (AMS) method. The Lanczos method uses the recursive formula to obtain the vector group, converts it into a triangular matrix, and then obtains the eigenvectors. The Subspace method uses the iterative method, and the AMS method has higher requirements on the mesh quality of the model. The results of the above three methods are all equally accurate. However, the Lanczos method requires less computation and faster computation speed than the latter two methods. In view of the large number of meshes in this model, the complex shape and structure, and the low quality of some meshes, it is more appropriate to use the Lanczos method to extract the modes in this paper. The modalities of the model were extracted by ABAQUS software, and the structural performance evaluation of the smart street lamp appearance design based on Kansei engineering designed in this paper is carried out through simulation research, and the results are obtained as shown in Table 1.

From the above research, it can be seen that the appearance design method of smart street lamps based on Kansei engineering proposed in this paper can effectively improve the structural performance of street lamps.

4. Conclusion

Considering that wind load is one of the main factors affecting the structural safety of smart street lamps, there have also been accidents in which street lamps have collapsed or broken due to wind disasters. It also increases the wind-receiving area and increases the accident probability of street lights in strong wind environments. Therefore, it is of far-reaching significance to study the wind resistance performance of smart street lights under the action of strong wind, evaluate their safety and ensure their safe operation, and further expand the market of smart street lights. This paper combines Kansei engineering to study the appearance design method of smart street lamps to improve the appearance design effect of street lamps. Moreover, this paper verifies that the intelligent street lamp design based on Kansei engineering meets the lighting needs through experimental research. Through the experimental evaluation, it can be seen that the appearance design method of smart street lamps based on Kansei engineering proposed in this paper can effectively improve the structural performance of street lamps.

Data Availability

The labeled dataset used to support the findings of this study are available from the corresponding author upon request.

Conflicts of Interest

The authors declare no conflicts of interest regarding the publication of this paper.

References

[1] G. Jia, G. Han, A. Li, and J. Du, "SSL: smart street lamp based on fog computing for smarter cities," *IEEE Transactions on Industrial Informatics*, vol. 14, no. 11, pp. 4995–5004, 2018.

[2] G. Gagliardi, M. Lupia, G. Cario et al., "Advanced adaptive street lighting systems for smart cities," *Smart Cities*, vol. 3, no. 4, pp. 1495–1512, 2020.

[3] S. Liu and M. Shao, "Based on big data LED smart street lighting system," *International Core Journal of Engineering*, vol. 5, no. 12, pp. 105–108, 2019.

[4] J. J. Zhang, W. H. Zeng, S. L. Hou, Y. Q. Chen, L. Y. Guo, and Y. X. Li, "A low-power and low cost smart streetlight system based on Internet of Things technology," *Telecommunication Systems*, vol. 79, no. 1, pp. 83–93, 2022.

[5] K. Sudheer, D. Madhurita, A. Chandana, M. Thanesh, and M. K. Babu, "Intelligent street light system for smart cities," *International Journal of Applied Science and Computations*, vol. 6, no. 5, pp. 684–690, 2019.

[6] H. P. Khandagale, R. Zambare, P. Pawar, P. Jadhav, P. Patil, and S. Mule, "Street light controller with GSM technology," *International Journal of Engineering Applied Sciences and Technology*, vol. 4, no. 10, pp. 268–271, 2020.

[7] R. Elavarasu and C. C. A. Rajan, "Solar powered Luo converter based smart street lighting using arduino UNO,"

International Journal of Pure and Applied Mathematics, vol. 118, no. 24, pp. 1–8, 2018.

[8] T. T. Ngo, P. H. Nguyen, D. H. Le Ta, H. M. Nguyen, T. D. Nguyen, and P. M. Le, "Development and implementation of smart street lighting system based on LoRa Technology," *Science & Technology Development Journal-Engineering and Technology*, vol. 2, no. 3, pp. 193–206, 2019.

[9] W. Brenner and N. Adamovic, "Creating sustainable photovoltaics for smart cities," *ENTRENOVA-ENTerprise REsearch InNOVAtion*, vol. 5, no. 1, pp. 457–461, 2019.

[10] M. S. Khan, A. Qadeem, F. Ali et al., "Movement aware smart street-lights for efficient energy utilisation: movement aware smart street-lights for efficient energy utilisation," *Proceedings of the Pakistan Academy of Sciences: A. Physical and Computational Sciences*, vol. 58, no. 1, pp. 77–84, 2021.

[11] H. S. Lee, B. W. Min, T. J. Yang, J. H. Eum, K. Kim, and J. Y. Lee, "A study on the concept and user perception of smart park-focused on the IoT see park users in Daegu City," *Journal of the Korean Institute of Landscape Architecture*, vol. 47, no. 5, pp. 41–48, 2019.

[12] L. Luo, "Data acquisition and analysis of smart campus based on wireless sensor," *Wireless Personal Communications*, vol. 102, no. 4, pp. 2897–2911, 2018.

[13] R. Mohamed, M. A. Mohamed, A. Ahmad, and M. Abd Halim, "Provisioning of street lighting based on ambience intensity for smart city," *Indonesian Journal of Electrical Engineering and Computer Science*, vol. 12, no. 3, pp. 1401–1406, 2018.

[14] S. Rajaram and B. Jayapalan, "Experimental and mathematical validation of power quality monitoring in smart cities using P/O luo converter fed solar PV array," *Dynamic Systems and Applications*, vol. 30, no. 10, pp. 1574–1584, 2021.

[15] R. Jia and W. Wu, "Case study on intelligent road lighting in foreign countries under the background of smart city," *Journal of Humanities and Social Sciences Studies*, vol. 4, no. 1, pp. 235–245, 2022.

[16] H. N. Lokhande and S. D. Markande, "Adaptive street light controlling for smart cities," *International Journal of Applied Engineering Research*, vol. 13, no. 10, pp. 7719–7723, 2018.

[17] O. Pribyl, P. Pribyl, M. Lom, and M. Svitek, "Modeling of smart cities based on ITS architecture," *IEEE Intelligent Transportation Systems Magazine*, vol. 11, no. 4, pp. 28–36, 2018.

[18] L. B. Imran, R. M. A. Latif, M. Farhan, and T. Tariq, "Real-time simulation of smart lighting system in smart city," *International Journal of Space-Based and Situated Computing*, vol. 9, no. 2, pp. 90–98, 2019.

[19] M. Hadipour, J. F. Derakhshandeh, and R. Rezaei, "Fully automatic cleaning system of smart street lights: a new design via Alf and vegard's RISC processor," *SN Applied Sciences*, vol. 2, no. 7, pp. 1–12, 2020.

[20] A. Senthil Kumar, G. Suresh, S. Lekashri, G. Babu Loganathan, and R. Manikandan, "Smart agriculture system with E–carbage using IoT," *International Journal of Modern Agriculture*, vol. 10, no. 1, pp. 928–931, 2021.

[21] M. Kanthi and M. Basil, "Wireless sensors network controlled smart street lighting system," *Journal of Advanced Research in Dynamical and Control Systems*, vol. 1, no. 13, pp. 805–812, 2018.